https://doi.org/10.1093/plphys/kiad519 PLANT PHYSIOLOGY 2023: 00: 1–11

Plant Physiology®

Research Article

Distinct ADP-ribosylation factor-GTP exchange factors govern the opposite polarity of 2 receptor kinases

Cecilia Rodriguez-Furlan [1,*] Ariana Emami [2] and Jaimie M. Van Norman [2,*]

1 School of Biological Sciences, Washington State University, Pullman, WA 99164, USA
2 Department of Botany and Plant Sciences, Center for Plant Cell Biology, Institute of Integrative Genome Biology, University of California, Riverside, Riverside, CA 92521, USA

*Author for correspondence: jaimie.vannorman@ucr.edu (J.M.V.N.), c.rodriguezfurlan@wsu.edu (C.R.-F.)
The authors responsible for distribution of materials integral to the findings presented in this article in accordance with the policy described in the Instructions for Authors (https://academic.oup.com/plphys/pages/General-Instructions) are Cecilia Rodriguez-Furlan and Jaimie M. Van Norman.

Abstract

Polarity of plasma membrane proteins is essential for cell morphogenesis and control of cell division and, thus, influences organ and whole plant development. In Arabidopsis (*Arabidopsis thaliana*) root endodermal cells, 2 transmembrane kinases, INFLORESCENCE AND ROOT APICES RECEPTOR KINASE (IRK) and KINASE ON THE INSIDE (KOIN), accumulate at opposite lateral domains. Their polarization is tightly linked to their activities regulating cell division and ground tissue patterning. The polarization of IRK and KOIN relies solely on the secretion of newly synthesized protein. However, the secretion machinery by which their opposite, lateral polarity is achieved remains largely unknown. Here, we show that different sets of ADP-ribosylation factor (ARF)-guanine-nucleotide exchange factors (ARF-GEFs) mediate their secretion. ARF-GEF GNOM-like-1 (GNL1) regulates KOIN secretion to the inner polar domain, thereby directing KOIN sorting early in the secretion pathway. For IRK, combined chemical and genetic analyses showed that the ARG-GEF GNL1, GNOM, and the BREFELDIN A-INHIBITED-GUANINE NUCLEOTIDE-EXCHANGE FACTORs 1 to 4 (BIG1-BIG4) collectively regulate its polar secretion. The ARF-GEF-dependent mechanisms guiding IRK or KOIN lateral polarity were active across different root cell types and functioned regardless of the protein's inner/outer polarity in those cells. Therefore, we propose that specific polar trafficking of IRK and KOIN occurs via distinct mechanisms that are not constrained by cell identity or polar axis and likely rely on individual protein recognition.

Introduction

Morphological and molecular asymmetries are fundamental properties of living cells. Polarized proteins are essential for normal cell structure and function, and polarized protein distribution is a hallmark of many biological systems (Gorelova et al. 2021). This polarization allows cells to change their shape, division orientation, and function attributes, which are foundational to tissue and organ development (Muroyama and Bergmann 2019). Using Arabidopsis (*Arabidopsis thaliana*) root as a model has aided cell polarization research (Guo and Dong 2022). The highly stereotyped cell divisions and resulting organization of cell layers lead to a clear polar distribution of cellular components along the root's principal axes: the rootward–shootward (basal/apical) axis and the inner–outer (lateral) axis. Therefore, polar localization of proteins along these axes delineates 4 distinct polar plasma membrane (PM) domains (Gorelova et al. 2021). Multiple proteins involved in critical physiological and developmental processes are known to be polarized to these distinct PM domains.

Among the described polarized proteins at the PM are the auxin efflux carriers PIN-FORMED (PIN) proteins, PIN2 and PIN1, which are oppositely polarized in the shootward–rootward axis (Raggi et al. 2020). PIN1 accumulates at the rootward PM domain in vascular and endodermal cells. Simultaneously, PIN2 is located at the shootward domain in epidermal and cortex cells and, together, they drive directional auxin flow, which is essential for root growth and

Received July 21, 2023. Accepted September 05, 2023. Advance access publication October 3, 2023

development. Also oppositely polarized but, in the inner–outer axis, are the leucine-rich repeat receptor-like kinases (LRR-RLKs), INFLORESCENCE AND ROOT APICES RECEPTOR KINASE (IRK), and KINASE ON THE INSIDE (KOIN; Campos et al. 2020; Rodriguez-Furlan et al. 2022). IRK shows polar accumulation in the outer PM domain in the endodermis and pericycle and the inner domain in epidermal and cortical cells. KOIN asymmetrically accumulates at the inner PM domain, toward the stele and opposite of IRK, in the endodermis and pericycle. IRK and KOIN are involved in repressing cell division in the root meristem. These 2 proteins, which are polarized on opposite sides of root endodermal and pericycle cells, are hypothesized to interpret bidirectional information to repress root cell proliferation.

The polar distribution of PM proteins is established, maintained, and/or dynamically altered mainly through endomembrane trafficking, which includes targeted secretion, endocytosis, and recycling (Marhava 2022). Distinct trafficking routes for shootward/rootward localization contribute to PIN1/PIN2 polarization (Kleine-Vehn et al. 2008b; Men et al. 2008; Li et al. 2017; Glanc et al. 2018). However, molecular players involved in the regulation of PIN1/PIN2-specific trafficking remain largely unidentified. One of the few proteins known to specifically regulate rootward traffic is the ADP-ribosylation factor (ARF)-guanine nucleotide-exchange factor (ARF-GEF) GNOM (Geldner et al. 2003; Zhang et al. 2020). After prolonged treatment with brefeldin A (BFA), a small molecule targeting sensitive ARF-GEFs, a rootward-to-shootward shift of PIN1 is observed, while the polarity of shootward localized PIN2 remains largely unchanged (Kleine-Vehn et al. 2006, 2008b). The BFA sensitivity or insensitivity of the 8 Arabidopsis ARF-GEFs is determined by a single amino acid in the Sec7 domain, which is the central catalytic domain (Geldner et al. 2003). BFA suppresses the function of GNOM and BFA-inhibited GEF (BIG) 1, BIG2, BIG4, BIG5, and GNOM-LIKE2 (GNL2; Fig. 1, A and B) but not that of BIG3 and GNOM-LIKE1 (GNL1; Tanaka et al. 2009; Richter et al. 2012, 2014; Kitakura et al. 2017; Xue et al. 2019). A weak mutant allele of *GNOM*, *gnom*^{R5}, demonstrated that GNOM affects PIN1 but not PIN2 trafficking (Kleine-Vehn et al. 2006, 2008b). Thus, GNOM action appears specifically linked to the PIN1 polarization pathway as BIG1, BIG2, BIG3, and BIG4 redundantly function in the trafficking of newly synthesized and endocytosed PINs to the PM (Richter et al. 2014).

The opposite, lateral (outer/inner) polarization of IRK and KOIN is also established through distinct pathways (Rodriguez-Furlan et al. 2022). Unlike PINs, their polarization does not depend on endocytosis and recycling but relies primarily on targeted secretion. IRK is trafficked through a BFA-sensitive secretion pathway, whereas KOIN is trafficked through a BFA-insensitive pathway. Here, we use a combination of chemical and genetic evidence to show that KOIN relies only on GNL1 for its inner polar localization, and regulation of its sorting likely occurs very early from the endoplasmic reticulum (ER). Distinctly, IRK secretion to the outer PM domain is regulated in concert by BFA-insensitive BIG3 and BFA-sensitive ARF-GEFs. Importantly, upon ectopic expression in the cortex and epidermis, we find that KOIN secretion to the inner PM domain remains GNL1 dependent and IRK secretion to the inner PM domain in these cells remains dependent on the same BFA-sensitive and BFA-insensitive ARF-GEFs that localize it to the outer domain in the endodermis. Our results indicate that the specific ARF-GEF activity regulating KOIN and IRK polarity in different root cell types is not linked to cell identity or a particular polarization axis but rather depends on protein identity. Our results thus reveal an increasingly complex regulatory framework for polar secretion in plant cells.

Results

BIG1-BIG4 are the primary ARF-GEFs regulating IRK secretion

Arabidopsis ARF-GEFs are essential regulators of vesicle formation and therefore of endomembrane trafficking. Among them, BIG1, BIG2, BIG4, BIG5, GNL2, and GNOM are sensitive to BFA, whereas GNL1 and BIG3 are BFA-insensitive (Fig. 1, A and B). Our analyses exclude GNL2, because it is only expressed during pollen development. IRK polar secretion in the root meristem is BFA-sensitive, whereas a BFA-insensitive secretion pathway is the primary contributor to KOIN polarity (Rodriguez-Furlan et al. 2022; Supplemental Fig. S1). Intriguingly, extended BFA treatment does not completely abolish IRK-GFP accumulation at the PM (Rodriguez-Furlan et al. 2022; Fig. 1, C, C′, H, and J). Likewise, IRK-GFP PM accumulation is only reduced and not abolished in the *big1,2,4* triple mutant (Fig. 1, D, D′, and E); yet, in *big1,2,4* mutants treated with BFA, IRK accumulation in BFA bodies is nearly abolished (Fig. 1, D, D′, F, and K). These data indicate that GNOM and BIG5 do not significantly contribute to IRK secretion and point to the contribution of BFA-insensitive ARF-GEFs to IRK secretion.

In the mutant of BFA-insensitive ARF-GEF, *BIG3*, we observed an 18% reduction in IRK accumulation at the PM (Fig. 1, G, G′, H, and L). Whereas IRK retention in BFA bodies was not affected in *big3* (Fig. 1, G, G′, and I). However, after 1 or 6 h of BFA treatment, a significant reduction in PM accumulation of IRK occurred in *big3* (Fig. 1, G and H). These results suggest BIG3 as the primary BFA-insensitive ARF-GEF involved in IRK polar secretion. Accordingly, IRK accumulation at the PM is reduced by ∼15% to 18% in the *big2,3,4*, *big1,3,4*, and *big1,2,3* triple mutants (Supplemental Fig. S2, A to E). After BFA treatment, the reduction in IRK PM accumulation in these triple mutants was comparable with that observed in *big3* alone (Supplemental Fig. S2, A′ to D′). Additionally, IRK retention in BFA bodies in these triples was significantly reduced (Supplemental Fig. S2, F to H), indicating an overall impairment of IRK secretion. Therefore, BIG1, BIG2, BIG3, and BIG4 have complementary functions in polar trafficking of newly synthesized IRK.

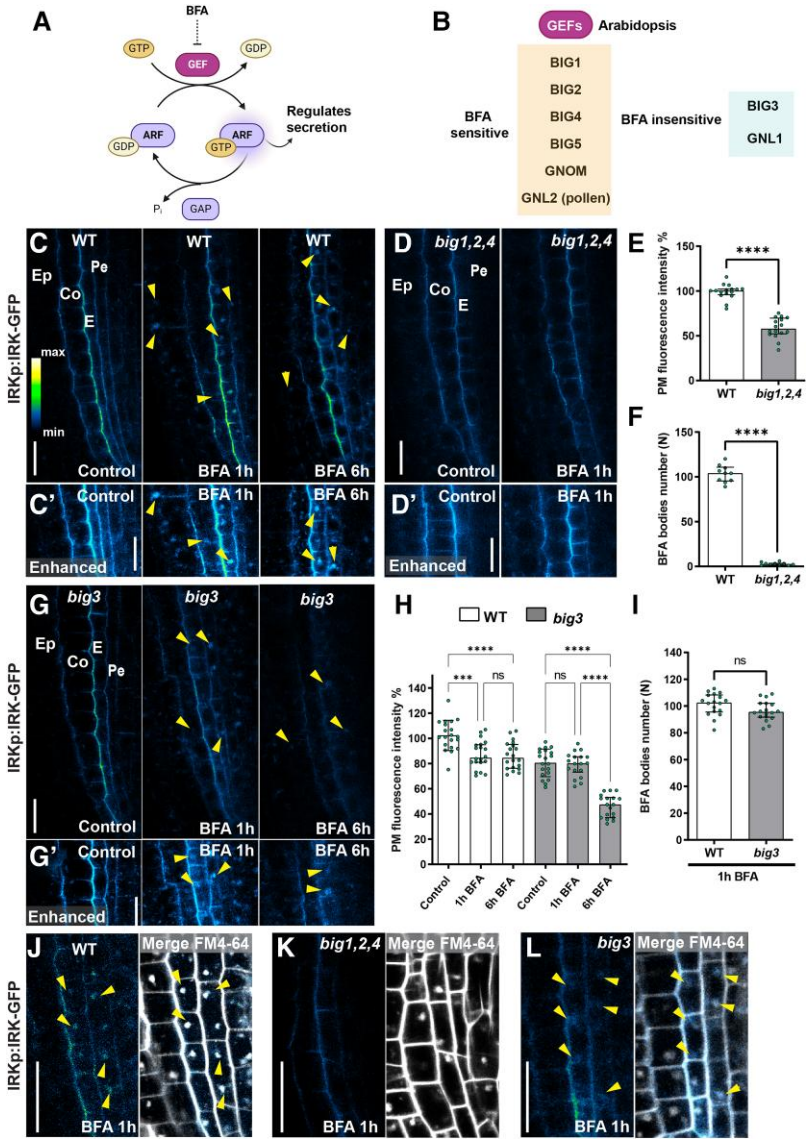

Figure 1. IRK polar secretion depends on the activity of BFA-sensitive and BFA-insensitive ARF-GEF BIG1-BIG4. **A)** Diagram showing the cycle of ARF family GTPase proteins during the exchange of GDP (guanosine diphosphate) to GTP (guanosine triphosphate), which is mediated by GEFs and the hydrolysis facilitated by GTPase-activating proteins (GAPs). Once bound to GTP, ARFs can interact with other proteins regulating protein secretion. **B)** The 8 Arabidopsis ARF-GEFs and their sensitivity to BFA. Diagrams (**A**, **B**) were generated with Biorender.com. **C)** Confocal micrographs of a portion of the root tip showing IRK-GFP accumulation, driven by the *IRK* promoter (*IRKp*) in WT, with controls and 50 μM BFA treatments for 1 and 6 h in panels from left to right. GFP alone is shown on an intensity scale. Cell types indicated: epidermis (Ep), cortex (Co), endodermis (E), pericycle (Pe). The arrowheads indicate BFA bodies. **C′)** Portions from panels shown in **C)** with enhanced brightness to highlight the intracellular BFA bodies. **D)** IRK-GFP signal in the BFA-inhibited GEF *(big)1,2,4* mutant in control and after 1 h BFA treatment, no BFA bodies are observed even with enhanced brightness **D′)**. **E)** Quantification of IRK-GFP fluorescence intensity at the PM in *big1,2,4* relative to the average for the WT controls expressed as a percentage. The dots show individual data points ($n = 20$ roots) per genotype per treatment and the bars indicate average fluorescence intensity. **F)** Quantification of BFA body number in *big1,2,4* relative to the average for the WT controls expressed as a percentage. **E and F)** Statistically significant differences assayed by using an unpaired *t*-test with Welch's correction test, with *P*-values indicated with asterisks: ****≤0.0001 and "ns" no statistically significant difference. Error bars indicate standard deviation (SD) **G)** IRK-GFP accumulation in *big3* with controls and BFA treatments for 1 and 6 h in panels from left to right. BFA bodies are dimmer than in WT but still observable, especially with enhanced brightness **G′)** as indicated by arrowheads. **H)** Quantification of IRK-GFP fluorescence intensity at the PM in WT and *big3* during BFA treatments and relative to their control conditions expressed in percentage ($n = 20$ roots per condition). Statistically significant differences assayed by 1-way ANOVA Tukey's multiple comparisons test, with *P*-values indicated with asterisks: ***0.002, ****0.0001, and "ns" indicates no statistically significant difference. The error bars indicate SD. **I)** Quantification of BFA body number in *big3* relative to the average for the WT controls expressed as a percentage. Statistical test as in **F)**, $n = 18$ roots per genotype. **J to L)** IRK-GFP (intensity scale, left panels) after 1 h BFA treatment in **J)** WT, **K)** *big1,2,4* triple mutant, and **L)** *big3* single mutants and with the merging of GFP and FM4-64 (gray scale) at right. The arrowheads point to BFA bodies and the scale bars indicate 20 μm in all panels.

The BFA-insensitive ARF-GEF, GNL1, regulates KOIN polar secretion

KOIN polar secretion in the root tip is largely controlled by a BFA-independent pathway (Rodriguez-Furlan et al. 2022; Supplemental Fig. S1, D to F). As expected, when expressed in the BFA-sensitive ARF-GEFs, *big1,2,4* triple mutant KOIN-GFP shows similar PM accumulation and polarization as it does in the wild type (WT; Fig. 2, A, B′, and D). BFA treatments in the *big1,2,4* mutant background disrupt activity of the remaining BFA-sensitive ARF-GEFs, BIG5, and GNOM. Again, as expected, KOIN-GFP accumulation at the PM in BFA-treated *big1,2,4* remains unchanged, and no KOIN fluorescence is observed in BFA bodies, which are detectable due to FM4-64 agglomerations (Fig. 2, A and B). These results indicate that KOIN secretion is likely controlled by BFA-insensitive ARF-GEFs.

The BFA-insensitive ARF-GEFs that could function in KOIN secretion are BIG3 and GNL1. We found that KOIN-GFP in *big3* exhibits PM accumulation comparable with that of WT controls (Fig. 2, A, A′, C, C′, and D). However, when KOIN is expressed in the *gnl1* mutant, its accumulation at the PM is reduced by nearly 80%, indicating that BFA-insensitive GNL1 activity largely regulates KOIN polar secretion (Fig. 2, E and F). Furthermore, when KOIN is expressed in the *gnl1-1* GNL1-BFAs (a BFA-sensitive point mutant) background (Richter et al. 2007), it can be detected in BFA bodies (Fig. 2G). Based on these findings, we propose that GNL1 is the main ARF-GEF-regulating KOIN secretion and that its activity alone has a major impact on the total accumulation of KOIN at the PM.

KOIN exit from the ER requires GNL1, but IRK ER exit is more complex and requires GNOM and GNL1

GNL1 is a BFA-insensitive ARF-GEF found in the Golgi and controls traffic between the ER and the Golgi (Richter et al. 2007; Teh and Moore 2007). In GNL1 mutants, the ARF-GEF activity regulating cargo traffic from the ER to the Golgi can be performed by the BFA-sensitive GNOM (Geldner et al. 2003; Richter et al. 2007; Naramoto et al. 2010). To investigate whether GNOM could also regulate KOIN secretion, we used BFA to inhibit GNOM activity in *gnl1-1*. However, we did not detect a further decrease in KOIN-GFP accumulation at the PM (Fig. 2, E and F). Our results collectively indicate that KOIN exit from the ER is specifically regulated by GNL1.

We then examined the role of GNL1 and GNOM in the regulation of IRK exit from the ER. Unlike KOIN-GFP, no reduction in PM accumulation of IRK-GFP was detected in *gnl1-1* roots (Fig. 3, A to D). However, substantially less IRK-GFP was detected at the PM after BFA treatment of *gnl1-1* (Fig. 3, E to H). By enhancing the image acquisition settings of *gnl1-1* roots treated with BFA for 1 h, we detected IRK retention in the ER, and longer BFA treatments increased ER retention (Fig. 3M), suggesting that GNOM contributes to the exit of IRK-GFP from the ER.

Retention of IRK in the ER was confirmed by co-localizing with an ER marker (Fig. 3N). To facilitate visualization, we expressed the ER marker only in endodermal cells, where PM accumulation of IRK-GFP is at its highest (Fig. 3N). To highlight the partial co-localization (Pearson's $r = 0.69$), we show an image where only the co-localizing GFP and ER-mCHERRY pixels are depicted (Fig. 3N, far right panel). These findings indicate that in the absence of GNL1, GNOM controls IRK exit from the ER, as described by Richter et al. (2007). Although GNOM has been implicated in ER–Golgi trafficking, it is possible that GNOM and GLN1 activities are required simultaneously for IRK to exit the ER. Since IRK secretion appears to depend on GNL1 but remains present at the PM, we further examined GNOM involvement by examining IRK presence at the PM in the *gnl1-1* GNL1-BFAs GN-BFAi (GNOM BFA-insensitive allele) background (Richter et al. 2007). After BFA treatment, IRK is retained in BFA bodies, while PM accumulation is reduced as expected but not to the same level observed after 1 h treatment in *gnl1-1* (Fig. 3, I to L). These results validate a role for GNOM in IRK secretion.

Overall, our findings identify GNL1 as the primary ARF-GEF-regulating KOIN ER exit from the ER, whereas control of IRK ER exit is likely more complex, requiring both GNL1 and GNOM.

Polarization of IRK and KOIN to the inner PM domain in cortex and epidermal cells is regulated by different ARF-GEFs

When expressed under their endogenous promoters, KOIN and IRK accumulate at opposite lateral domains in endodermal cells (Rodriguez-Furlan et al. 2022). Our previous findings, as well as those presented here, support the participation of distinct ARF-GEFs in the regulation of KOIN and IRK secretion to inner and outer polar domains in endodermal cells. In the literature, it has been extensively postulated that, by various partially understood mechanisms, the conserved ARF-GEF machinery is strongly associated with modulating protein secretion to different polar PM domains (Geldner et al. 2003; Kleine-Vehn et al. 2008a; Tanaka et al. 2009; Richter et al. 2010; Singh et al. 2018; Brumm et al. 2020). This suggests that particular ARF-GEFs may be associated with the polar distribution of KOIN to the inner PM domain, while others direct IRK to the outer PM domain. We, therefore, examined the impact of ARF-GEF regulation on IRK and KOIN when they are directed to the same lateral domain to determine whether their particular ARF-GEF regulation would be maintained.

To address this, we ectopically expressed KOIN in the cortex and epidermal cells using the *UBIQUITIN10* promoter (*UBQ10p*; Fig. 4, A, C, E, and G). In these cell types, both KOIN and IRK accumulate at the inner PM domain (Fig. 4, A, B, B′, C, and D, left panels). Upon BFA treatment, only IRK is found in BFA bodies in the epidermis and cortex, while KOIN secretion remains unaffected (Fig. 4, A, B, B′, C, and D right panels). Furthermore, in *gnl1-1*, the presence of KOIN at the PM of epidermis and cortex cells is greatly reduced,

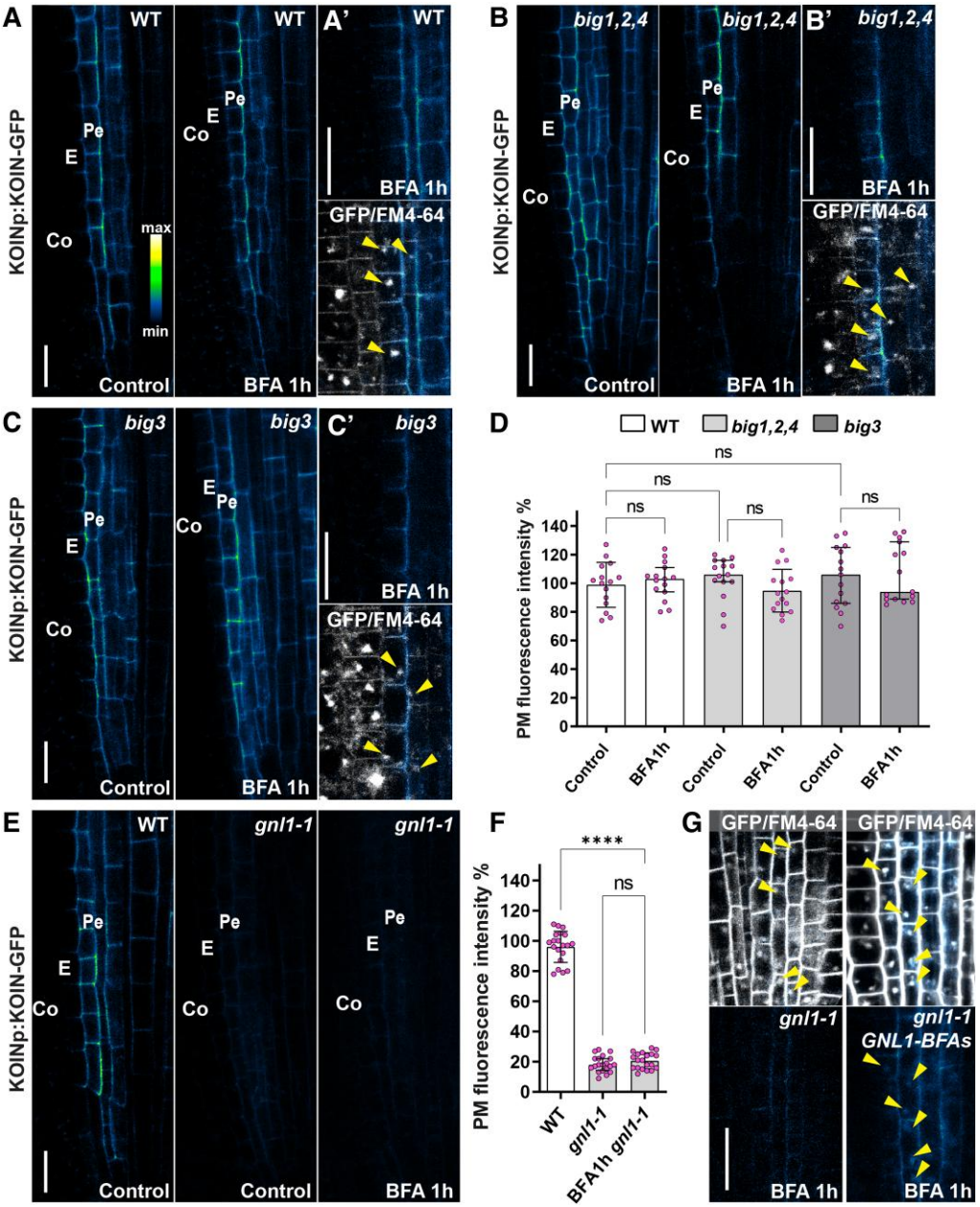

Figure 2. KOIN polar secretion and ER exit depend on the BFA-insensitive ARF-GEF GNL1. **A)** Confocal micrographs of a portion of the root tip showing KOIN-GFP accumulation, driven by the *KOIN* promoter (*KOINp*). Control panels (left) and BFA treatments (right) show GFP alone (intensity scale) and no BFA bodies are visible. **A′)** GFP alone (upper) and FM4-64 merged with GFP (lower panel). BFA bodies indicated with FM4-64 (arrowheads) do not show GFP accumulation. Cell types indicated: epidermis (Ep), cortex (Co), endodermis (E), and pericycle (Pe). **B)** KOIN-GFP accumulation in the BFA-inhibited GEF (*big)1,2,4* mutant in control (left) and 1 h BFA treatment (right) with no BFA bodies observed. **B′)** BFA bodies are visible as FM4-64 agglomerations (lower, arrowheads) but are devoid of KOIN-GFP (upper). **C)** KOIN-GFP in the *big3* mutant in control (left) and 1 h BFA treatments (right). **C′)** FM4-64 accumulates in BFA bodies in *big3* (lower), but those accumulations do not have GFP signal (upper). **D)** Quantification of KOIN-GFP fluorescence intensity at the PM after 1 h BFA treatment in WT, *big1,2,4* and *big3* relative to their control conditions expressed as percentage. The circles show individual data points ($n = 20$ roots) per genotype per treatment and the bars indicate average fluorescence intensity. Statistically significant differences assayed by using the 1-way ANOVA Tukey's multiple comparisons test, with *P*-values indicated with asterisks: ****0.0001, and "ns" no statistically significant difference. The error bars are SD. **E)** KOIN-GFP in WT and *gnl1-1* in control conditions (left) and *gnl1-1* 1 h BFA treatments (right). **F)** Quantification of KOIN-GFP fluorescence intensity at the PM in WT, *gnl1-1*, and *gnom-like1-1* (*gnl1-1)* after BFA treatment relative to WT control conditions and expressed as percentage. Statistical analysis similar to **D)**. The error bars indicate SD. **G)** FM4-64 (gray scale) merged with KOIN-GFP (intensity scale) (upper) and KOIN-GFP alone (lower) and after 1 h BFA treatment in (left) *gnl1-1* and (right) *gnl1-1* GNL1-BFAs (s, sensitive). Arrowheads indicate BFA bodies in the endodermis and pericycle. The scale bars for all panels are at 20 μm.

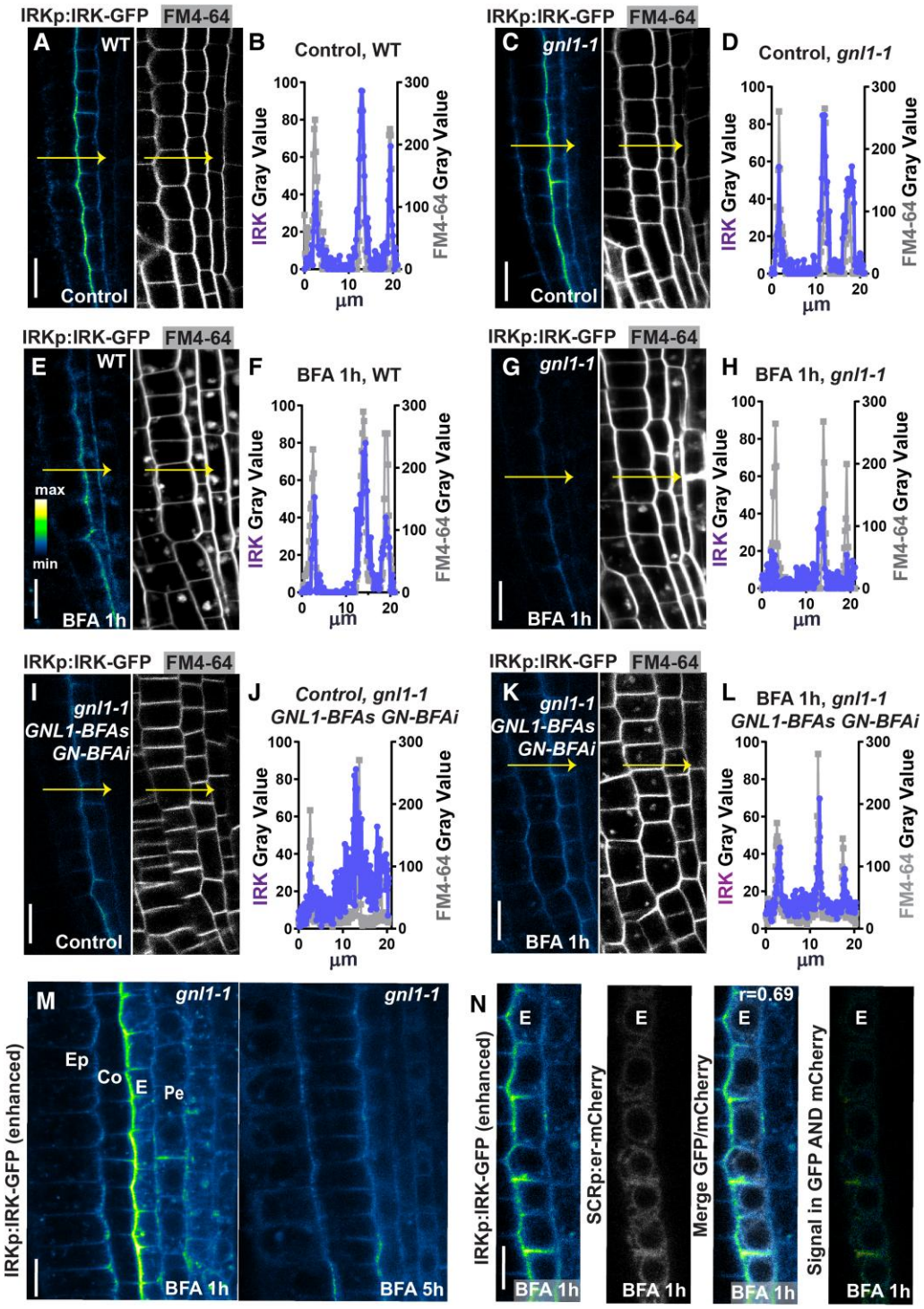

Figure 3. GNL1 is required for IRK exit from the ER. **A)** Confocal micrographs of a portion of the WT root tip showing IRK-GFP accumulation driven by the IRK promoter (*IRKp*; left, with intensity scale) and FM4-64 fluorescence (right, gray scale). **B)** Quantification of IRK-GFP fluorescence (circles) and FM4-64 (squares) intensity at a single line (arrows in **A**) from the epidermis inward to the pericycle (measured as distance). **C and D)** IRK-GFP and FM4-64 fluorescence and quantification at the PM in *gnl1-1*. **E and F)** IRK-GFP and FM4-64 fluorescence and quantification in WT and **G and H)** *gnl1-1* treated with BFA and their line quantification. Note the decrease IRK-GFP at the PM, while the FM4-64 signal is unchanged. **I and J)** IRK-GFP and FM4-64 fluorescence and quantification in *gnom-like1-1* (*gnl1-1*) mutants expressing GNL1-BFA sensitive (BFAs) and GN-BFA insensitive (BFAi) in control conditions and **K and L)** after 1 h BFA treatment. **M)** A portion of *gnl1-1* root tips treated with BFA over time using enhanced image acquisition settings to show GFP intracellular signal. **N**, left to right) In *gnl1-1*, IRK-GFP alone intensity color scale enhanced to show signal, ER-mCHERRY alone (gray scale), the IRK-GFP + ER-mCHERRY merged, and (far right) IRK-GFP and ER-mCHERRY co-localization only (phase intensity scale). The cell types indicated: epidermis (Ep), cortex (Co), endodermis (E), pericycle (Pe). Scale bars: 20 μm, except **N)** at 10 μm.

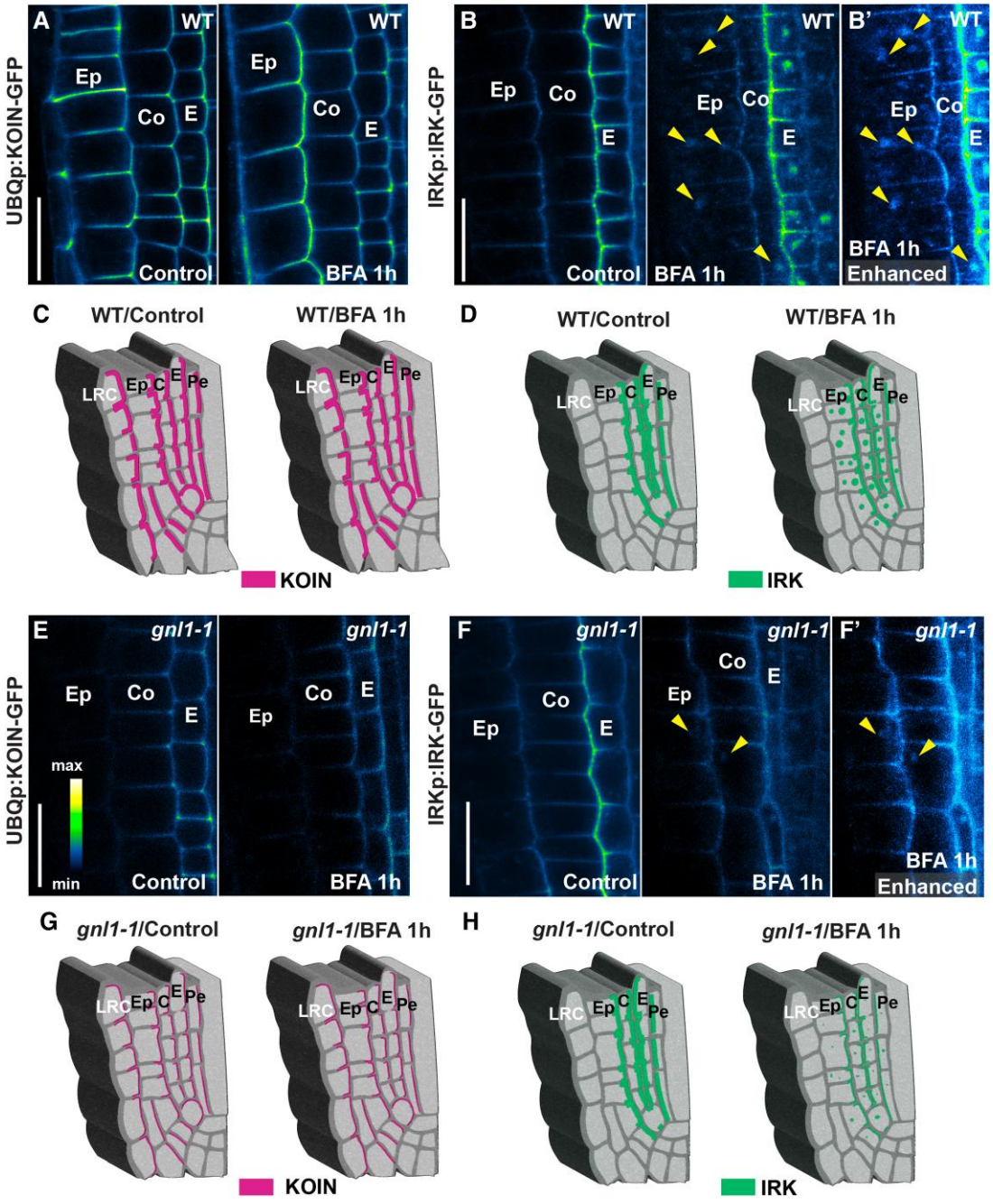

Figure 4. IRK and KOIN secretion to the inner polar domain is regulated by different ARF-GEFs. **A)** Confocal micrographs of a portion of root tips showing KOIN-GFP accumulation (intensity scale) in several cell types, among them the epidermis and cortex, when expressed by the *UBQUITIN10* promoter (*UBQ10p*) in WT under control (left) and 1 h BFA treatment (right) conditions. Note that no BFA bodies are visible at the epidermis or cortex. **B)** IRK-GFP expression driven by the IRK promoter (*IRKp*) is detectable at the PM of epidermis and cortex cells in WT under control (left) and BFA treatment (right) conditions. Note that dim BFA bodies are visible in the epidermis and cortex with **B′)** enhanced brightness to better visualize BFA bodies (arrowheads) in these cells. **C and D)** Schematics of a root tip portion showing inner polar accumulation of KOIN **C)** and the inner/outer accumulation of IRK **D)** in different cell types in under (left) control and (right) BFA treatment conditions. **E)** KOIN-GFP accumulation in the epidermis and cortex upon expression from *UBQ10p* in *gnl1-1* control (left) and BFA treatment (right) conditions. Note that KOIN PM accumulation is lower in the epidermal and cortex cells in *gnl1-1* but do not change after 1 h BFA treatment. **F)** IRK-GFP accumulation in *gnl1-1* control (left) and BFA treatment (right) conditions. Note that BFA bodies are observed in WT **B and B′**, right panel) but not in *gnl1-1* **F)** with IRK PM accumulation diminishing only after BFA treatment in *gnl1-1*. BFA bodies are present (right panel, arrowheads) and are more noticeable when the image brightness is enhanced **F′)**. **G and H)** Schematics of a root tip portion showing inner polar accumulation of KOIN **E)** or the inner/outer accumulation of IRK **F)** in different cell types in *gnl1-1* under (left) control and (right) BFA treatment conditions. Cell types indicated the following: lateral root cap (LRC), epidermis (Ep), cortex (Co), endodermis (E), pericycle (Pe). Scale bars: 20 μm.

whereas IRK accumulation at the PM remains unchanged (Fig. 4, E and F, F′, G, and H, left panels). It is only upon treatment with BFA in *gnl1-1* that IRK accumulation is reduced at the PM in the epidermis and cortex, whereas KOIN accumulation is unchanged (Fig. 4, E, F, F′, G, and H, right panels).

Thus, ARF-GEF-mediated control of KOIN/IRK secretion is tissue-independent and the activity of a specific ARF-GEF does not restrict these proteins to a single polar PM domain. These findings suggest that the ARF-GEF-dependent machinery regulating PM accumulation of KOIN and IRK is protein specific rather than associated with secretion toward a particular axis or polar PM domain.

Discussion

How PM proteins acquire and maintain their polarity is a fundamental biological question. Multiple studies indicate a variety of post-Golgi mechanisms including hyperpolar secretion, clathrin-mediated endocytosis (Kitakura et al. 2011), polar recycling (Geldner et al. 2003; Kitakura et al. 2011), lipid raft-dependent restriction of lateral diffusion (Willemsen et al. 2003; Jaillais and Gaude 2008; Men et al. 2008), and protein phosphorylation (Huang et al. 2010; Zhang et al. 2010) influence PM membrane protein polarity. It is generally thought that rootward (basally)-localized auxin transporters take a different route during sorting than their shootward (apically)-localized counterparts (Kleine-Vehn et al. 2008a; Li et al. 2017). Despite this, one of the few proteins known to specifically regulate PIN recycling to the rootward PM domain is the ARF-GEF GNOM (Geldner et al. 2003). This suggests the mechanisms underlying protein localization to specific polar domains remain unclear.

In endodermal cells, the LRR-RLK IRK and KOIN exhibit opposite polarity to the inner and outer PM domains, respectively. Our previous results showed that KOIN and IRK polarization at the PM was mainly dependent on polarized secretion. Inhibition of ARF-GEF activity by BFA led us to conclude that IRK secretion was BFA sensitive, whereas KOIN secretion was BFA insensitive (Rodriguez-Furlan et al. 2022). Additionally, pretreatments with the protein synthesis inhibitor cycloheximide followed by co-treatment with BFA-depleted IRK-GFP from BFA bodies indicate that the GFP signal resulted from the disruption of newly synthesized IRK secretion. Here, we investigated which ARF-GEFs regulate the polar secretion of these receptors. We discovered an IRK trafficking route that is specifically regulated by the ARF-GEF BIG1-BIG4. We concluded that the influence of BIG5 on IRK secretion is negligible after analyzing different combinations of *big* mutants and BFA treatments. These findings are consistent with the previously characterized activities of BIG1-BIG4 in regulating bulk protein secretion (Richter et al. 2014). During secretion, BIG1-BIG4 operate as functionally overlapping ARF-GEFs, controlling the production of AP-1 complex–coated transport vesicles required for late-secretory trafficking from the trans-Golgi-Network (TGN) to the PM. Consistently, our findings support complementary roles for BIG1-BIG4 in regulating the secretion of newly synthesized IRK to the lateral PM domains. The requirement for BIG1-BIG4 in IRK secretion appears to be required regardless of cell identity and does not restrict IRK localization to a particular lateral domain.

Although the activity of BIG1-BIG4 is linked to the regulation of bulk protein secretion (Richter et al. 2014), we show that BIG family members do not regulate KOIN secretion. This suggests that KOIN secretion is independent of the AP-1 complex–coated transport pathway. Therefore, KOIN polar secretion appears to be mediated by a yet-uncharacterized BFA-independent secretion mechanism. In this way, KOIN emerges as a remarkable protein marker for studying alternative secretion pathways that are independent of BIG1-BIG4 regulation.

Furthermore, we previously demonstrated that during cytokinesis, IRK—but not KOIN—is found at the nascent PM membrane (Rodriguez-Furlan et al. 2022). In conjunction with our findings, BIG1-BIG4-dependent bulk secretion is described to guide proteins to the nascent PM during cell division (Richter et al. 2014). Consequently, our current analyses contribute to explaining why IRK but not KOIN are localized to this new membrane.

The BFA-insensitive KOIN secretion pathway is independent of BIGs and GNOM, but it depends on the ARF-GEF activity of GNL1. Accordingly, KOIN cannot reach the inner PM domain in the *gnl1-1* mutant despite GNOM activity in these plants. GNL1, a Golgi-resident protein, controls the early secretory pathway by mediating the COPI recycling of ER-resident proteins from the Golgi back to the ER. When *gnl1-1* plants are treated with BFA, ER–Golgi trafficking collapses because COPI coat complexes cannot be recruited to the cis-Golgi membrane (Richter et al. 2007). Therefore, evidence indicates that KOIN exit from the ER is primarily GNL1 dependent.

It has been reported that BFA-sensitive GNOM plays a role in ER–Golgi trafficking in addition to its role in recycling and that PIN1 traffic is GNL1/GNOM dependent at the early secretory pathway (Doyle et al. 2015). Due to their important and broad role in secretion, *gnl1-1* mutants are dwarves and hypersensitive to BFA, with a complete inhibition of root growth when compared with the WT when grown with BFA. Consistently, BFA treatment in *gnl1-1* resulted in IRK retention at the ER. Therefore, unlike KOIN, IRK exit from the ER is dependent on both GNL1 and GNOM. These results suggest differential sorting for IRK and KOIN in the ER early on in the secretory pathway.

This differential sorting would likely utilize other components of vesicle trafficking pathways, like particular SNARE complexes. These complexes are assembled on the ER and transported as cis-SNARE complexes (rather than monomeric SNARE proteins) through the Golgi stacks and the TGN to the nascent membrane during cell division, where they are transformed into trans-SNARE complexes that target vesicles to the PM (Karnahl et al. 2017). Intriguingly, the SNARE complex VAMP721/722-SYP121-SNAP33 is retained at the ER in a GNL1-dependent manner. Future work can determine

whether KOIN associates with the SNARE complex VAMP721/722-SYP121-SNAP33 in the ER and is co-transported to the Golgi and TGN, where the SNARE complex directs its fusion specifically to the inner PM domain by a BIG1-BIG4-independent mechanism. We have previously shown that KOIN secretion is ES16 sensitive (Rodriguez-Furlan et al. 2022), and RAB GTPase A 2A (RABA2A) is a known ES16 target (Li et al. 2017). RABA2A interacts with the VAMP721/722-SYP121-SNAP33 SNARE complex, thereby directing the shootward-polarized secretion of PIN2 (Pang et al. 2022). It would be interesting to determine whether KOIN associates with the SNARE complex VAMP721/722-SYP121-SNAP33 to direct its polar localization to the inner PM domain and to evaluate whether expressing a dominant negative soluble fragment of these SNAREs affects KOIN secretion.

An early association of KOIN with a cis-SNARE complex at the ER could sort it into Golgi and TGN subdomains, thus resulting in inner polar localization that is independent of root cell type. In contrast, the IRK secretion pathway likely allows shifts in polar localization between the inner PM domain in the epidermis and cortex and the outer PM domain in the endodermis and pericycle. In both cases, the ARF-GEF-dependent secretion mechanisms appear specific to each of these LRR-RLKs. Interestingly, the secretion of the LRR-RLK ERECTA-LIKE1 and the RLK FERONIA can be modulated at the ER by the interaction with chaperones or glycosylphosphatidylinositol-anchored proteins (Li et al. 2015; Yang et al. 2022). Both ERECTA-LIKE 1 and FERONIA are retained in the ER in the absence of these ER proteins. Therefore, evidence suggests that tight regulation of ER exit is part of the secretion mechanism of several RLKs.

Collectively, our results present additional information on the mechanisms driving the polarization of LRR-RLKs in root cell types. These mechanisms likely involve early sorting of KOIN and IRK at the ER that sets up distinct polar secretion paths for each. These findings reveal avenues for research focused on identifying specific molecular complexes that direct polarized protein traffic to the PM.

Materials and methods

Plant material and growth conditions

Arabidopsis (*A. thaliana*) materials utilized here are Columbia-0 (Col-0, WT) and previously described reporter and mutants: *IRKp:IRK-GFP* (Campos et al. 2020), *KOINp:KOIN-GFP* (Rodriguez-Furlan et al. 2022); *gnl1-1*, *gnl1-1 BFAs*, and *gnl1-1 BFAs GN-BFAi* (the former 2 genotypes received from Dr Gerd Jüergens, University of Tuebingen, Richter et al. 2007); and the *big* mutants: *big3*, *big1,2,3*, *big1,3,4*, *big1,2,4*, and *big2,3,4* (Richter et al. 2014). The *IRKp:IRK-GFP* and/or *KOINp:KOIN-GFP* expression vectors were transformed (as described below) or crossed into the backgrounds of *gnl1-1*, *gnl1-1 BFAs*, *gnl1-1 BFAs GN-BFAi*, *big3*, *big1,2,3*, *big1,3,4*, *big1,2,4*, or *big2,3,4* by standard approaches. The *KOINp:KOIN-GFP* expression vector was transformed into the backgrounds of *gnl1-1* and *big3*. The *SCRp-ER-mCHERRY* expression vector was transformed into *IRKp:IRK-GFP gnl1-1* plants.

Prior to growth in a percival growth chamber maintained at a constant temperature of 22 °C with 16/8 h illumination regime, seeds were surface-sterilized with chlorine gas. Dry seeds in open tubes were placed in a closed chamber in a fume hood and exposed to the gas for 1 to 4 h, which was generated by mixing 100 mL household bleach with 3 mL HCl (10 Normal). Sterile seeds were then sown on solid growth medium containing 1× Murashige and Skoog basal salts (Caisson Labs), 0.5 g/L MES, 1% w/v sucrose, and 1% w/v agar (Difco). After stratification in the dark at 4 °C for at least 48 h, seedlings were cultivated for 4 to 7 d on vertically oriented plates sealed with micropore tape prior to imaging/analysis.

Plasmid construction

Invitrogen Multisite Gateway Technology (Carlsbad, CA, USA) was used to generate expression vectors as previously described. Briefly, previously generated pENTR vectors (Campos et al. 2020; Rodriguez-Furlan et al. 2022) were recombined into destination vectors to create expression vectors for plant transformation. Expression vectors generated for these experiments: *UBQp:KOIN-GFP* (pGreen-BarT backbone), *KOINp:KOIN-GFP* (pGreen-NorfT backbone), and *SCRp:ER-mCherry* (pP7m34GW backbone).

Generation of transgenic plants

Expression vectors were validated by Sanger sequencing and introduced into *Agrobacterium tumefaciens* strain GV3101 containing the *pSOUP* helper plasmid. Expression vectors were transformed into WT, *gnl1-1*, *big3*, *big1,2,3*, *big1,3,4*, *big1,2,3,4*, or *IRKp:IRK-GFP gnl1-1* plants by the floral dip method (Clough and Bent 1998). Standard methods were used to select transformed plants with Basta resistance (dpGreen-BarT) or Norflurazon (dpGreen-NorfT) as previously described (Campos et al. 2020; Rodriguez-Furlan et al. 2022). T2 lines with a resistant-to-sensitive ratio of 3:1, indicating a single locus insertion, were chosen for propagation. T3 progeny with 100% resistant seedlings (homozygous) was chosen for further study. At least 3 independent lines for each reporter were examined for this study, all having consistent fluorescence and protein-reporter distribution. For the selection of *IRKp:IRK-GFP gnl1-1* transformed with *SCRp:ER-mCherry*, T1 seeds were screened for seed coat GFP fluorescence (Wang et al. 2020), using a blue light source and a dissecting microscope. All the T1 seeds selected were positive for the transgene, and further selection was carried out using a similar approach as described above.

Chemical treatments

Seedlings were grown for 5 to 6 d poststratification on 1× MS solid medium plates sealed with tape. Seedlings were transferred to 24-well plates (10 seedlings per well) containing 1 mL of 1× MS liquid medium and treated for up to 6 h with 50 μM BFA or the solvent control. A stock solution of 50 mM BFA (Sigma-Aldrich) was prepared using DMSO as a solvent. Imaging was performed in a 1× MS liquid medium

including the respective chemical or solvent control. At least 20 plants per condition were analyzed per treatment, and the experiments were replicated at least 3 times to ensure reproducibility. Representative results are shown.

Confocal microscopy and image analysis

The PM of root cells was visualized by staining roots with 10 μM FM4-64 (Thermo-Fisher) diluted in liquid 1× MS medium for 5 to 10 min. Images were taken using a Leica SP8 upright confocal microscope with a water-corrected 40× objective. The pinhole was set at 1 airy unit for each wavelength, and system parameters were set as follows: GFP excitation 488 nm, emission collected at 492 to 530 nm; mCherry excitation 594 nm, emission collected at 585 to 660 nm; and FM4-64 excitation 488 nm, emission collected at 600 to 660 nm. Fluorescent protein signals were collected with the HyD detector with gain at 70% to 100%, while other signals (PI) were detected with the PMT detector with a gain set between 500 and 700. When acquiring fluorescence data from the same root for both GFP and mCh or FM4-64, in-line sequential scanning was utilized to prevent signal bleeding through. Images were processed with either the LAS X software or exported and processed in ImageJ (imagej.nih.gov/ij/).

Signal intensity of IRK-GFP and KOIN-GFP was quantified in ImageJ using the Measure tool and applying the formula: corrected signal intensity = integrated density − (area selected × mean fluorescence of background readings). Additionally, the Fiji ImageJ plugin Peripheral was utilized to quantify the PM signal in accordance with Vosolsobě et al. (2018) to avoid quantifying cytoplasmic agglomerations. Control values were used as a reference to generate a percentage of signal intensity when compared with the respective control treatment. The 2D graphs displaying IRK-GFP pixel intensities across a portion of the root (arrows) were generated with the plot profile plugin in ImageJ. The *x* axis represents the distance of the line drawn across the root tissues, and the *y* axis is the pixel intensity along that line.

For each quantification, the raw data were exported to excel, and the graphic output was produced using Prism (GraphPad, San Diego, CA, USA).

Accession numbers

Sequence data from this article can be found in the GenBank/EMBL data libraries under the following: accession numbers IRK (NM_115495) and KOIN (NM_001345296). Sequence data used in this article can be found in the Arabidopsis Information Resource (https://www.arabidopsis.org/index.jsp) under the following accession numbers: AT3G56370 (IRK), AT5G58300 (KOIN).

Acknowledgments

The authors thank all the members of the Van Norman's laboratory for discussions of the project and feedback on the manuscript while it was in preparation. The authors thank Jessica Toth and Roya Campos for assisting with the selection of the *UBQp:KOIN-GFP* transgenic plants.

Author contributions

C.R.-F. and J.M.V.N.: conceptualization. C.R.-F., A.E., and J.M.V.N.: methodology and investigation. C.R.-F. and J.M.V.N.: resources. C.R.-F.: writing—original draft. C.R.-F. and J.M.V.N.: writing—review and editing. C.R.-F.: visualization. J.M.V.N. and C.R.-F.: supervision. J.M.V.N.: funding acquisition.

Supplemental data

The following materials are available in the online version of this article.

Supplemental Figure S1. IRK polar secretion is BFA sensitive, while KOIN polar secretion is resistant to BFA treatment.

Supplemental Figure S2. IRK secretion is compromised in *big* triple mutants.

Funding

Work for the initial version of the manuscript was funded by USDA-NIFA-CA-R-BPS-5156-H and a NSF CAREER award #1751385 to J.M.V.N. and work for the revised manuscript was also funded by start-up funds to C.R.-F. from Washington State University.

Conflict of interest statement. None declared.

References

Brumm S, Singh MK, Nielsen ME, Richter S, Beckmann H, Stierhof Y-D, Fischer A-M, Kumaran M, Sundaresan V, Jürgens G. Coordinated activation of ARF1 GTPases by ARF-GEF GNOM dimers is essential for vesicle trafficking in Arabidopsis. Plant Cell. 2020:**32**(8):2491–2507. https://doi.org/10.1105/tpc.20.00240

Campos R, Goff J, Rodriguez-Furlan C, Van Norman JM. The Arabidopsis receptor kinase IRK is polarized and represses specific cell divisions in roots. Dev Cell. 2020:**52**(2):183–195.e4. https://doi.org/10.1016/j.devcel.2019.12.001

Clough SJ, Bent AF. Floral dip: a simplified method for Agrobacterium-mediated transformation of Arabidopsis thaliana. Plant J. 1998:**16**(6):735–743.

Doyle SM, Haeger A, Vain T, Rigal A, Viotti C, Łangowska M, Ma Q, Friml J, Raikhel NV, Hicks GR, et al. An early secretory pathway mediated by GNOM-LIKE 1 and GNOM is essential for basal polarity establishment in *Arabidopsis thaliana*. Proc Natl Acad Sci U S A. 2015:**112**(7):E806–E815. https://doi.org/10.1073/pnas.1424856112

Geldner N, Anders N, Wolters H, Keicher J, Kornberger W, Muller P, Delbarre A, Ueda T, Nakano A, Jürgens G. The Arabidopsis GNOM ARF-GEF mediates endosomal recycling, auxin transport, and auxin-dependent plant growth. Cell. 2003:**112**(2):219–230. https://doi.org/10.1016/S0092-8674(03)00003-5

Glanc M, Fendrych M, Friml J. Mechanistic framework for cell-intrinsic re-establishment of PIN2 polarity after cell division. Nat Plants. 2018:**4**(12):1082–1088. https://doi.org/10.1038/s41477-018-0318-3

Gorelova V, Sprakel J, Weijers D. Plant cell polarity as the nexus of tissue mechanics and morphogenesis. Nat Plants. 2021:**7**(12):1548–1559. https://doi.org/10.1038/s41477-021-01021-w

Guo X, Dong J. Protein polarization: spatiotemporal precisions in cell division and differentiation. Curr Opin Plant Biol. 2022:**68**:102257. https://doi.org/10.1016/j.pbi.2022.102257

Huang F, Kemel Zago M, Abas L, van Marion A, Galván-Ampudia CS, Offringa R. Phosphorylation of conserved PIN motifs directs Arabidopsis PIN1 polarity and auxin transport. Plant Cell. 2010:**22**(4):1129–1142. https://doi.org/10.1105/tpc.109.072678

Jaillais Y, Gaude T. Plant cell polarity: sterols enter into action after cytokinesis. Dev Cell. 2008:**14**(3):318–320. https://doi.org/10.1016/j.devcel.2008.02.007

Karnahl M, Park M, Mayer U, Hiller U, Jürgens G. ER assembly of SNARE complexes mediating formation of partitioning membrane in Arabidopsis cytokinesis. Elife. 2017:**6**:e25327. https://doi.org/10.7554/eLife.25327

Kitakura S, Adamowski M, Matsuura Y, Santuari L, Kouno H, Arima K, Hardtke CS, Friml J, Kakimoto T, Tanaka H. BEN3/BIG2 ARF GEF is involved in brefeldin A-sensitive trafficking at the trans-Golgi network/early endosome in *Arabidopsis thaliana*. Plant Cell Physiol. 2017:**58**(10):1801–1811. https://doi.org/10.1093/pcp/pcx118

Kitakura S, Vanneste S, Robert S, Löfke C, Teichmann T, Tanaka H, Friml J. Clathrin mediates endocytosis and polar distribution of PIN auxin transporters in Arabidopsis. Plant Cell. 2011:**23**(5):1920–1931. https://doi.org/10.1105/tpc.111.083030

Kleine-Vehn J, Dhonukshe P, Sauer M, Brewer PB, Wiśniewska J, Paciorek T, Benková E, Friml J. ARF GEF-dependent transcytosis and polar delivery of PIN auxin carriers in Arabidopsis. Curr Biol. 2008a:**18**(7):526–531. https://doi.org/10.1016/j.cub.2008.03.021

Kleine-Vehn J, Dhonukshe P, Swarup R, Bennett M, Friml J. Subcellular trafficking of the Arabidopsis auxin influx carrier AUX1 uses a novel pathway distinct from PIN1. Plant Cell. 2006:**18**(11):3171–3181. https://doi.org/10.1105/tpc.106.042770

Kleine-Vehn J, Łangowski Ł, Wiśniewska J, Dhonukshe P, Brewer PB, Friml J. Cellular and molecular requirements for polar PIN targeting and transcytosis in plants. Mol Plant. 2008b:**1**(6):1056–1066. https://doi.org/10.1093/mp/ssn062

Li C, Yeh FL, Cheung AY, Duan Q, Kita D, Liu MC, Maman J, Luu EJ, Wu BW, Gates L, et al. Glycosylphosphatidylinositol-anchored proteins as chaperones and co-receptors for FERONIA receptor kinase signaling in Arabidopsis. Elife. 2015:**4**:e06587.

Li R, Rodriguez-Furlan C, Wang J, van de Ven W, Gao T, Raikhel NV, Hicks GR. Different endomembrane trafficking pathways establish apical and basal polarities. Plant Cell. 2017:**29**(1):90–108. https://doi.org/10.1105/tpc.16.00524

Marhava P. Recent developments in the understanding of PIN polarity. New Phytol. 2022:**233**(2):624–630. https://doi.org/10.1111/nph.17867

Men S, Boutté Y, Ikeda Y, Li X, Palme K, Stierhof Y-D, Hartmann M-A, Moritz T, Grebe M. Sterol-dependent endocytosis mediates post-cytokinetic acquisition of PIN2 auxin efflux carrier polarity. Nat Cell Biol. 2008:**10**(2):237–244. https://doi.org/10.1038/ncb1686

Muroyama A, Bergmann D. Plant cell polarity: creating diversity from inside the box. Annu Rev Cell Dev Biol. 2019:**35**(1):309–336. https://doi.org/10.1146/annurev-cellbio-100818-125211

Naramoto S, Kleine-Vehn J, Robert S, Fujimoto M, Dainobu T, Paciorek T, Ueda T, Nakano A, Van Montagu MC, Fukuda H, et al. ADP-ribosylation factor machinery mediates endocytosis in plant cells. Proc Natl Acad Sci U S A. 2010:**107**(50):21890–21895. https://doi.org/10.1073/pnas.1016260107

Pang L, Ma Z, Zhang X, Huang Y, Li R, Miao Y, Li R. The small GTPase RABA2a recruits SNARE proteins to regulate the secretory pathway in parallel with the exocyst complex in Arabidopsis. Mol Plant. 2022:**15**(3):398–418. https://doi.org/10.1016/j.molp.2021.11.008

Raggi S, Demes E, Liu S, Verger S, Robert S. Polar expedition: mechanisms for protein polar localization. Curr Opin Plant Biol. 2020:**53**:134–140. https://doi.org/10.1016/j.pbi.2019.12.001

Richter S, Anders N, Wolters H, Beckmann H, Thomann A, Heinrich R, Schrader J, Singh MK, Geldner N, Mayer U, et al. Role of the GNOM gene in Arabidopsis apical-basal patterning—from mutant phenotype to cellular mechanism of protein action. Eur J Cell Biol. 2010:**89**(2–3):138–144. https://doi.org/10.1016/j.ejcb.2009.11.020

Richter S, Geldner N, Schrader J, Wolters H, Stierhof Y-D, Rios G, Koncz C, Robinson DG, Jürgens G. Functional diversification of closely related ARF-GEFs in protein secretion and recycling. Nature. 2007:**448**(7152):488–492. https://doi.org/10.1038/nature05967

Richter S, Kientz M, Brumm S, Nielsen ME, Park M, Gavidia R, Krause C, Voss U, Beckmann H, Mayer U, et al. Delivery of endocytosed proteins to the cell–division plane requires change of pathway from recycling to secretion. Elife. 2014:**3**:e02131. https://doi.org/10.7554/eLife.02131

Richter S, Müller LM, Stierhof Y-D, Mayer U, Takada N, Kost B, Vieten A, Geldner N, Koncz C, Jürgens G. Polarized cell growth in Arabidopsis requires endosomal recycling mediated by GBF1-related ARF exchange factors. Nat Cell Biol. 2012:**14**(1):80–86. https://doi.org/10.1038/ncb2389

Rodriguez-Furlan C, Campos R, Toth JN, Van Norman JM. Distinct mechanisms orchestrate the contra-polarity of IRK and KOIN, two LRR-receptor-kinases controlling root cell division. Nat Commun. 2022:**13**(1):235. https://doi.org/10.1038/s41467-021-27913-1

Singh MK, Richter S, Beckmann H, Kientz M, Stierhof YD, Anders N, Fäßler F, Nielsen M, Knöll C, Thomann A, et al. A single class of ARF GTPase activated by several pathway-specific ARF-GEFs regulates essential membrane traffic in Arabidopsis. PLoS Genet. 2018:**14**(11):e1007795. https://doi.org/10.1371/journal.pgen.1007795

Tanaka H, Kitakura S, De Rycke R, De Groodt R, Friml J. Fluorescence imaging-based screen identifies ARF GEF component of early endosomal trafficking. Curr Biol. 2009:**19**(5):391–397. https://doi.org/10.1016/j.cub.2009.01.057

Teh O, Moore I. An ARF-GEF acting at the Golgi and in selective endocytosis in polarized plant cells. Nature. 2007:**448**(7152):493–496. https://doi.org/10.1038/nature06023

Vosolsobě S, Schwarzerová K, Petrášek J, Vosolsobě S, Schwarzerová K, Petrášek J. Determination of plasma membrane partitioning for peripherally-associated proteins. J Vis Exp. 2018:**136**:57837. https://doi.org/10.3791/57837-v

Wang X, Ye L, Lyu M, Ursache R, Löytynoja A, Mähönen AP. An inducible genome editing system for plants. Nat Plants. 2020:**6**(7):766–772. https://doi.org/10.1038/s41477-020-0695-2

Willemsen V, Friml J, Grebe M, van den Toorn A, Palme K, Scheres B. Cell polarity and PIN protein positioning in Arabidopsis require STEROL METHYLTRANSFERASE1 function. Plant Cell. 2003:**15**(3):612–625. https://doi.org/10.1105/tpc.008433

Xue S, Zou J, Liu Y, Wang M, Zhang C, Le J. Involvement of BIG5 and BIG3 in BRI1 trafficking reveals diverse functions of BIG-subfamily ARF-GEFs in plant growth and gravitropism. Int J Mol Sci. 2019:**20**(9):2339. https://doi.org/10.3390/ijms20092339

Yang KZ, Zuo CR, Leng YJ, Yue JL, Liu HC, Fan ZB, Xue XY, Dong J, Chen LQ, Le J. The functional specificity of ERECTA-family receptors in Arabidopsis stomatal development is ensured by molecular chaperones in the endoplasmic reticulum. Development. 2022:**149**(17):dev200892.

Zhang J, Nodzyński T, Pěnčík A, Rolčík J, Friml J. PIN phosphorylation is sufficient to mediate PIN polarity and direct auxin transport. Proc Natl Acad Sci U S A. 2010:**107**(2):918–922. https://doi.org/10.1073/pnas.0909460107

Zhang X, Adamowski M, Marhava P, Tan S, Zhang Y, Rodriguez L, Zwiewka M, Pukyšová V, Sánchez AS, Raxwal VK, et al. Arabidopsis flippases cooperate with ARF GTPase exchange factors to regulate the trafficking and polarity of PIN auxin transporters. Plant Cell. 2020:**32**(5):1644–1664. https://doi.org/10.1105/tpc.19.00869

Supplemental Data

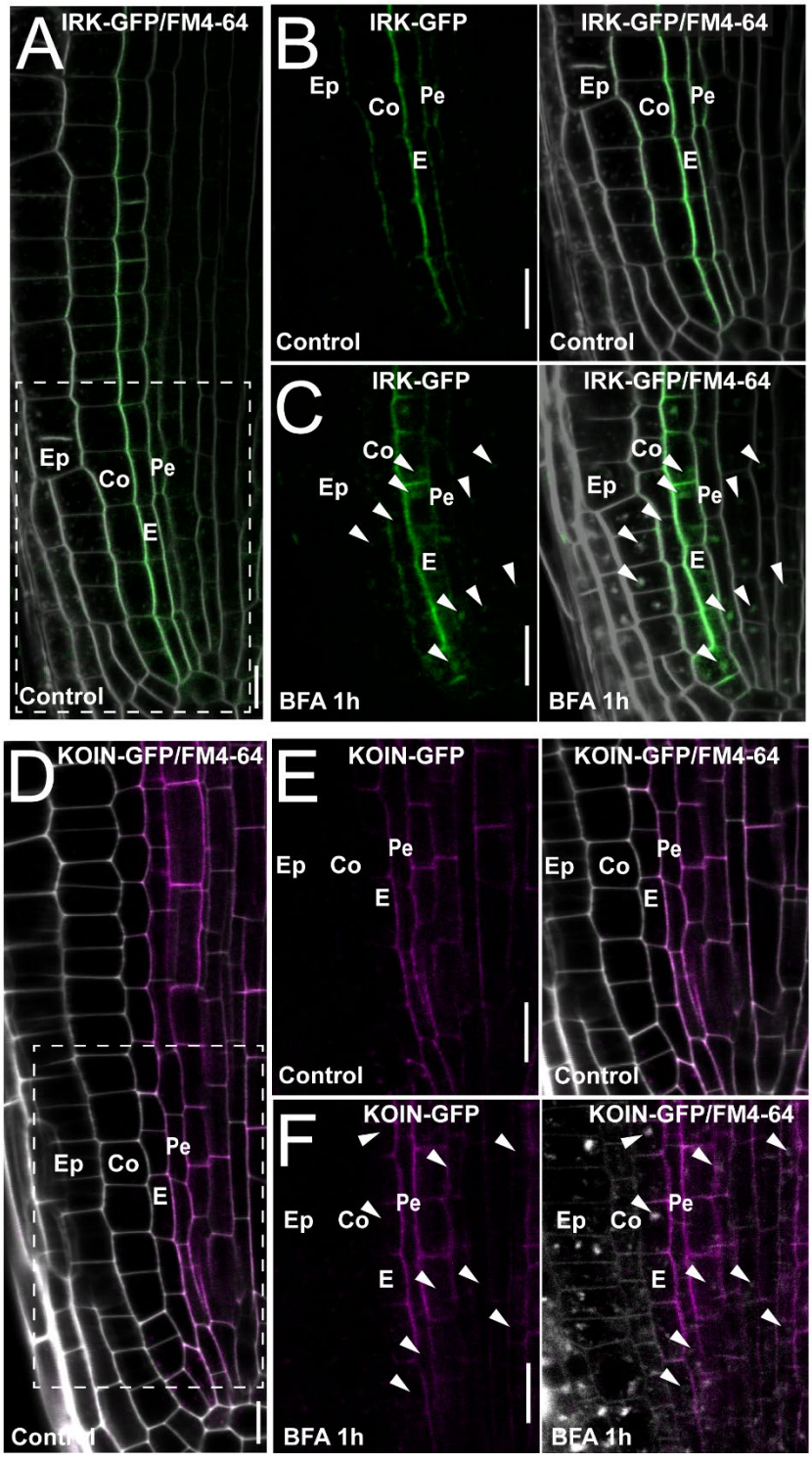

Supplemental Figure S1. IRK polar secretion is BFA sensitive, while KOIN polar secretion is resistant to BFA treatment. Confocal micrographs of a portion of wild type root meristems expressing (A-C) INFLORESCENCE AND ROOT APICES RECEPTOR KINASE (IRK)-GFP and (D-F) KINASE ON THE INSIDE (KOIN)-GFP from their endogenous promoters. (A, D) Images of control roots showing GFP (IRK in green and KOIN in magenta) and plasma membrane marker FM4-64 (white). Boxed areas indicate the region of the root tip shown in B and E, respectively. (B, C, E, F) GFP image alone (left) and GFP+FM4-64 merged (right) in (B, E) control roots and (C, F) roots treated with Brefeldin A (BFA) for 1 hour. Note in (F) BFA bodies do not appear in the KOIN-GFP only image. Cell types indicated: epidermis (Ep), cortex (Co), endodermis (E), pericycle (Pe). Arrowheads indicate BFA bodies and scale bars indicate 20 μm.

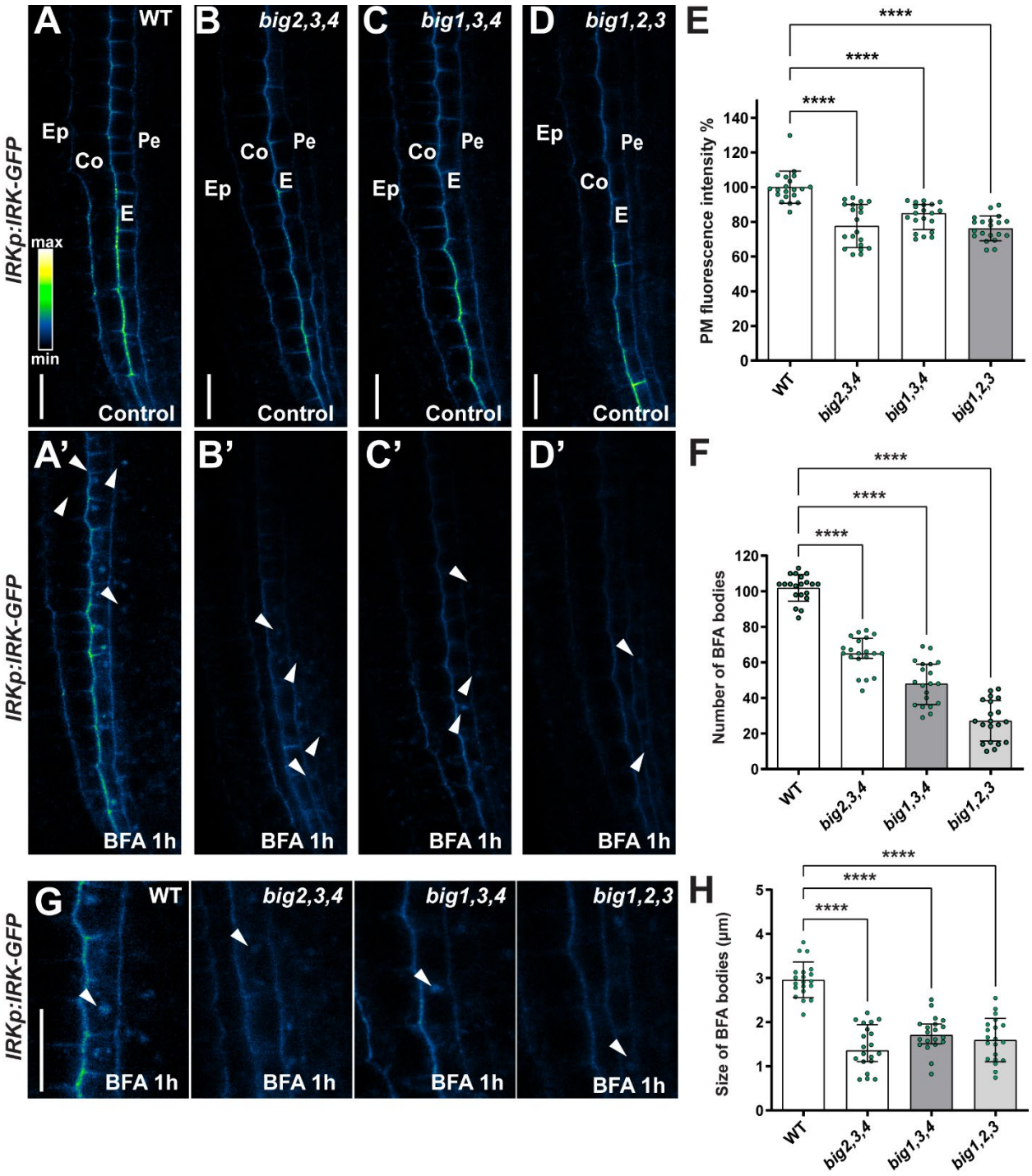

Supplemental Figure S2. IRK secretion is compromised in *brefeldin A-inhibited guanine nucleotide-exchange factor* (*big)* triple mutants. (A-D) Confocal micrographs of the root tip showing INFLORESCENCE AND ROOT APICES RECEPTOR KINASE (IRK)-GFP accumulation, driven by *IRKp* in (A) WT and (B) *big2 big3 big4,* (C) *big1 big3 big4*, (D) *big1 big2 big3* triple mutants, with (A-D) controls and

(A’-D’) 1 h Brefeldin A (BFA) treatments. GFP alone is shown with color intensity scale. (E) Quantification of IRK-GFP fluorescence intensity at the PM upon 1h BFA treatment relative to average for WT. Green dots show individual data points (n = 20 roots) per genotype and bars indicate average fluorescence intensity. (F) BFA body quantification upon BFA treatment in WT and triple mutant genotypes (n = 20 roots per genotype). (G) Image of BFA body size in the endodermis of WT and the various *big* triple mutants (from left to right). (H) Quantification of BFA body size between WT and triple mutant genotypes upon BFA treatment. Cell types indicated: epidermis (Ep), cortex (Co), endodermis (E), pericycle (Pe). Arrowheads indicate BFA bodies and scale bars indicate (A-D’) 20 µm and (G) 10 µm. One-way Anova Dunn's multiple comparisons test, with p-values indicated with asterisks: **** < 0.0001 *** < 0.001, and ‘ns’ = no statistically significant difference. Error bars indicate standard deviation (SD).